Int. J. Electrochem. Sci., 14 **(2019)** 8080 – 8096, doi: 10.20964/2019.08.88

International Journal of
ELECTROCHEMICAL
SCIENCE
www.electrochemsci.org

Corrosion Inhibition Effect of Tungstate on Fine-Grain High-Strength Reinforcement in Simulated Concrete Pore Solutions Containing Chloride Ions

Bilan Lin[1,2,*], *Xiaojuan Liu*[1] *and Yuye Xu*[3,*]

[1] School of Material Science and Engineering, Xiamen University of Technology, Xiamen, 361024 Fujian, China
[2] Key Laboratory of Functional Materials and Applications of Fujian Province, Xiamen, 361024 Fujian, China
[3] College of Civil Engineering, Huaqiao University, Xiamen, 361021 Fujian, China
[*]E-mail: linbilan@xmut.edu.cn; yuyexu@hqu.edu.cn

Received: 28 November 2018 / *Accepted:* 9 February 2019 / *Published:* 30 June 2019

Tungstate and tungstate/tartrate inhibitors were used to mitigate the corrosion of fine-grain high-strength (FGHS) reinforcement in simulated concrete pore solutions containing 3.5% NaCl. The physical laws governing the inhibition were investigated using potentiodynamic polarization and electrochemical impedance spectroscopy. The semiconductor characteristics of the corrosion products were analyzed by plotting the Mott–Schottky curves and the corrosion morphology was observed using SEM. A comparison with conventional carbon steel reinforcement (HPB300 steel) was also performed. The results indicated that tungstate is an anodic corrosion inhibitor. Sodium tungstate at concentrations between 0.1 and 0.3 g/L provided good corrosion inhibition, decreasing the corrosion current density from 12.3 $\mu A \cdot cm^{-2}$ to 0.326 $\mu A \cdot cm^{-2}$. The carrier density of the corrosion product layer and the electric double-layer capacitance decreased dramatically, while the charge transfer resistance improved significantly. Furthermore, only a few pits formed on the FGHS reinforcement. The tungstate/tartrate mixed inhibitor was found to display the advantages of a single inhibitor, although no synergistic effect was observed. When the inhibitor was absent, the corrosion resistance properties of FGHS reinforcement were clearly inferior to those of HPB300 steel. However, the addition of tungstate or tungstate/tartrate mixed inhibitor led to improved indicators of corrosion resistance for the FGHS sample relative to HPB300 steel.

Keywords: Reinforcement; Corrosion; Inhibitor; Tungstate; Electrochemical corrosion

1. INTRODUCTION

Grain refinement is considered an ideal strengthening mechanism as it affords significant improvements in both the strength and ductility of materials. Precipitation strengthening is another

commonly used strengthening mechanism despite causing a slight loss of ductility. Based on the optimum design for grain refinement and precipitation strengthening, FGHS) reinforcement offers high strength and good ductility, and thus has been widely used to produce reinforced concrete structures for use in both mild environments and harsh coastal environments [1–3]. Recently, a great deal of research has been conducted to determine the mechanical properties of FGHS reinforcement and the load capacity and seismic performance of FGHS-reinforced concrete structures, etc. [4–6]. However, literature regarding the corrosion behavior of FGHS reinforcement remains quite limited [7,8].

The reinforcement is in a passivation state in uncontaminated concrete due to its high alkalinity. However, the passivation film on the surface of the reinforcement can be damaged by the action of chloride ions originating from the environment, leaving the reinforcement in an active state [9–11]. Chloride ions are one of the predominant species responsible for the corrosion of reinforced structures [11–13].

The corrosion associated with reinforcement is classified as electrochemical corrosion, and is closely related to the uniformity of the surface state, the chemical composition, and the grain structure [9,10]. In many cases such as metallographic corrosion, the potential of the grain boundary is lower than that of the grain. Thus, the former can act as the anode of a corrosion cell, which causes anodic dissolution [9,10]. Compared with HPB300 reinforcement, the area of the grain boundaries is larger in FGHS reinforcement, leading to greater sensitivity to corrosion by chloride ions [14,15]. Shi et al. [15,16] pointed out that there are more grain boundaries and more grain boundary inclusions in fine-grain steel and these are the main reasons for its poorer corrosion resistance with respect to chloride ions in a concrete medium. Torbati-Sarraf et al. [9] coupled thermomechanically treated (TMT) steel, which was produced by a thermomechanical control process and contained fine grains, with carbon steel in a concrete medium containing chloride ions, and found that the TMT steel acted as the anode owing to its low corrosion resistance. In previous studies [17–19], the corrosion inhibition effects of phosphate, nitrate, and molybdate on FGHS reinforcement were clearly less than those on HPB300 reinforcement.

The use of corrosion inhibitors is one of the three major protection methods for metals [10,20], and these have also been widely applied in reinforced concrete structures [21–24]. Tungstate is an environmentally friendly corrosion inhibitor [25–27]. Although tungstate possesses lower oxidation power than chromate or nitrate [28], it still provides good corrosion inhibition effect for steel when a concentration of 0.3 g/L is attained [29]. Fe^{2+} can be oxidized to Fe^{3+} by tungstate, and the tungstate is concomitantly reduced to a lower valence state [30–32]. The stability and corrosion resistance of the aforementioned reaction products are high. Moreover, tungstate promotes the adsorption of oxygen atoms onto metal surfaces [32]. Sastri et al. [33] found that tungstate afforded similar corrosion inhibition to chromate in a coal–water slurry. Fujioka et al. [34] reported that competitive adsorption of tungstate ions and chloride ions occurs, leading to the displacement of some of the chloride ions. The adsorption of tungstate anions makes the film prefer cations, obstructing the adsorption and removal of chloride anions. Mu et al. [35] found that a small amount of tungstate is beneficial for the formation of a polytungstate salt, which is readily adsorbed on the surface of the metal and subsequently also inhibits the adsorption of chloride ions. Abedin [36] reported that the adsorption of tungstate ions on defects or pits was the main factor responsible for corrosion inhibition. Liu et al. [37] suggested that

tungstate acts mainly as a repair membrane instead of the main body; thus, the concentration of tungstate inhibitor can be quite low. In addition, numerous studies have reported that tungstate mixed inhibitor can further enhance the corrosion resistance of carbon steel or stainless steel [38–40]. Jabeera et al. [41] demonstrated that although tartrate itself accelerates the corrosion of carbon steel, a synergistic effect of corrosion resistance was achieved when tungstate and tartrate were used in a 1:1 ratio. Lu et al. [42] found that the inhibitory effect of tungstate was poor at pH 6–7 but markedly improved under alkaline conditions. However, the influence of tungstate on the corrosion of reinforced steels has not yet been reported.

In this study, the pH of the simulated concrete pore (SCP) solution was approximately 12.5. Tungstate was selected as a corrosion inhibitor for FGHS reinforcement, and the inhibitory effect of a tungstate/tartrate mixed inhibitor was evaluated. Differences in inhibition between FGHS reinforcement and HPB300 reinforcement were also investigated.

2. EXPERIMENTAL

2.1 Materials and reagents

The diameters of the FGHS and HPB300 reinforcement specimens were 16 and 12 mm, respectively. The microstructure was composed of white ferrite and black pearlite in both cases, although the grain size was clearly smaller in the FGHS reinforcement than in the HPB300 reinforcement, as shown in Fig. 1.

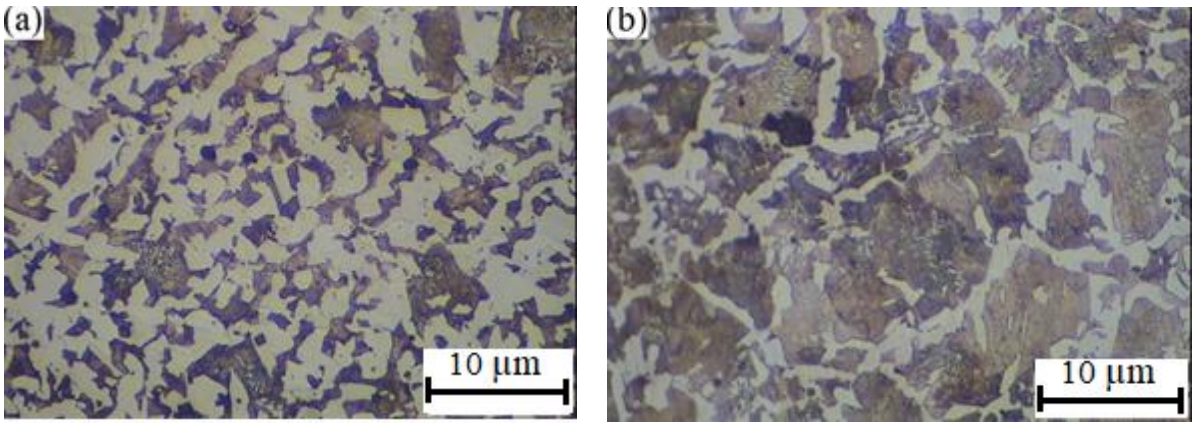

Figure 1. Optical micrograph structure of (a) FGHS reinforcement and (b) HPB300 reinforcement.

A saturated calcium hydroxide solution was used as the SCP solution. The sodium chloride content was 3.5%. The concentrations of the sodium tungstate inhibitor were 0, 0.05, 0.1, 0.3, 0.5, and 1.0 g/L. The mixed inhibitor was prepared from sodium tungstate and sodium tartrate in a concentration ratio of 1:1, such that the content of sodium tartrate and sodium tungstate was 0.1 g/L. All of the test solutions were prepared using analytical grade reagents and distilled water.

2.2 Electrochemical measurements

The reinforcement samples (5 mm thick) were cut using a precision cutting machine. One end of the sample served as the working face and the other end was welded to a copper conductor. Except for the working face, all parts of the samples were sealed with epoxy resin. The working areas for the FGHS and HPB300 reinforcement samples were 2.01 and 1.13 cm^2, respectively. Prior to testing, the working faces of the samples were ground in a sequential manner with metallographic papers (from No. 200 to No. 2000). The samples were then scrubbed with acetone, rinsed with distilled water, and dried with cold air.

Potentiodynamic polarization curves, electrochemical impedance spectroscopy (EIS) measurements, and Mott–Schottky curves were recorded. The electrochemical measurements were performed in a three-electrode system. A saturated calomel electrode (SCE) and a platinum electrode served as the reference and auxiliary electrodes, respectively, while the working electrode was the test specimen. Prior to the electrochemical measurements, the reinforcement sample was immersed in the SCP solution for 1 h to obtain a stable open-circuit potential.

Potentiodynamic polarization tests were commenced from the cathodic direction. The initial potential was the open-circuit potential minus 0.3 V. The anodic polarization was stopped when the anodic polarization current increased rapidly with polarization potential. The scan rate was 1 mV/s.

The EIS measurements were conducted at the open-circuit potential. The frequency ranged from 100 kHz to 0.01 Hz, and the signal amplitude was 5 mV. The EIS data were fitted using the ZView software.

The Mott–Schottky curves were obtained using the impedance–potential technique. The potential was in the range of −0.6 to 0.6 V *vs*. SCE. The amplitude and frequency of the AC signal were 10 mV and 1000 Hz, respectively. The potential step at the working electrode was 10 mV. The semiconductor characteristics of the corrosion products on the surfaces of the reinforcement samples were determined according to Mott–Schottky theory [43,44].

2.3 Microscopic analysis

The test specimens were ground sequentially with metallographic papers (No. 200 to No. 2000). The samples were then scrubbed with acetone, rinsed with distilled water, and dried with cold air. Finally, the samples were immersed in the SCP solutions for 5 h, followed by rinsing with distilled water and drying with cold air. The morphologies and chemical compositions of the corroded specimens were examined using SEM and energy-dispersive X-ray spectroscopy (EDS), respectively.

3. RESULTS AND DISCUSSION

3.1 Influence of tungstate concentration on FGHS reinforcement corrosion

Figure 2 shows the effects of sodium chloride and sodium tungstate on the corrosion morphology of FGHS reinforcement. In pure SCP solution, the passivation film on the surface of the FGHS sample was continuous and complete. In the presence of 3.5% NaCl, the corrosion products

were bubbled or even cracked and the film became very coarse, indicating severe corrosion of the FGHS sample. After the addition of the tungstate inhibitor, almost no bubbles or cracks formed, although there were still a small number of pits. The EDS results demonstrated the presence of a substantial amount of chloride within the bubbles and cracks, whereas chloride was not detected in the continuous film. Therefore, the bubbling and cracking of the corrosion product film was ascribed to the participation of chloride ions in the film formation. Moreover, tungsten was not observed in the EDS analysis, suggesting a very low concentration of tungstate in the film.

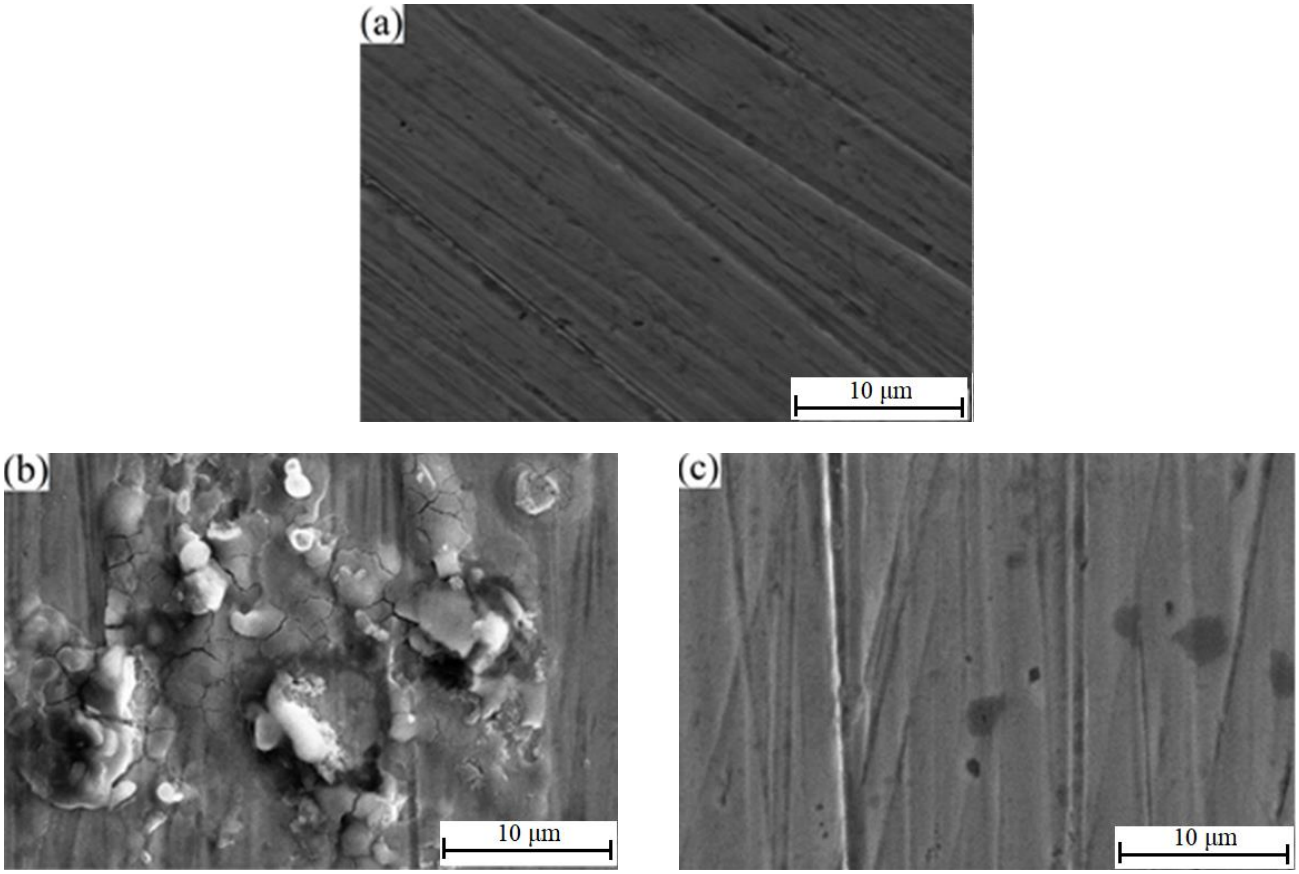

Figure 2. Corrosion morphology of FGHS reinforcement in SCP solutions: (a) uncontaminated, (b) with 3.5% NaCl, (c) with 3.5% NaCl and sodium tungstate inhibitor.

Figure 3 shows the influence of various concentrations of sodium tungstate on the polarization curves of FGHS reinforcement samples in SCP solutions containing 3.5% NaCl. The corresponding polarization parameters are listed in Table 1. P_e is the corrosion protection efficiency of tungstate and can be expressed as

$$P_e(\%) = (1 - i_{corr} / i_{corr}^0) \times 100\%$$

where i_{corr} and i_{corr}^0 are the corrosion current densities of the FGHS reinforcement in SCP solutions with and without sodium tungstate, respectively [10,45].

As shown in Fig. 3, in the SCP solutions containing 3.5% NaCl but no sodium tungstate, the anodic and cathodic polarization curves for the FGHS reinforcement exhibited the characteristics of

activation polarization. The resistance to the electrode reactions at both the anode and cathode originated mainly from charge transfer. That is, the electron flow rate, including the flow migration to the anode and the flow supply of the cathode, was the slowest step of the electrode reaction. In general, a series of dissolution reactions of the metal into the electrolyte is characteristic of activation polarization. This indicates that FGHS reinforcement in SCP solution containing 3.5% NaCl undergoes an active dissolution process.

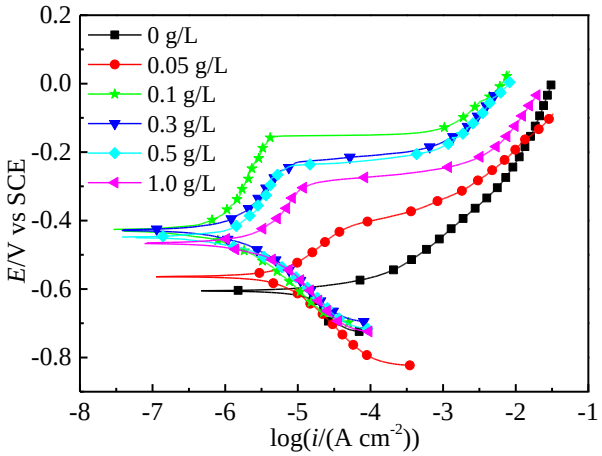

Figure 3. Effect of sodium tungstate concentration on polarization curves for FGHS reinforcement in SCP solutions containing 3.5% NaCl.

Table 1. Effect of sodium tungstate concentration on the polarization parameters of FGHS reinforcement in SCP solutions containing 3.5% NaCl.

Sodium tungstate concentration/g L^{-1}	i_{corr}/μA·cm^{-2}	E_{corr}/V *vs.* SCE	E_b/V *vs.* SCE	P_e/%
0	12.3	−0.605	-	-
0.05	1.46	−0.564	-	88.1
0.1	0.326	−0.428	−0.15	97.3
0.3	0.437	−0.428	−0.23	96.4
0.5	0.458	−0.449	−0.24	96.3
1.0	0.490	−0.485	−0.29	96.0

As shown in Fig. 3, in the presence of sodium tungstate inhibitor, the cathodic polarization curves changed little, whereas the anodic curves shifted to the left by various degrees. The characteristics of activation polarization control gradually diminished. However, the effect of concentration polarization control became stronger and some of the anodic curves even exhibited a small passivation region. Thus, tungstate acted as an anodic corrosion inhibitor. Upon increasing the sodium tungstate concentration from 0 g/L to 0.1 g/L, the anodic polarization current of the FGHS reinforcement decreased drastically, whereas it increased at higher concentrations.

As shown in Table 1, upon increasing the concentration of sodium tungstate, the corrosion current density (i_{corr}) of the FGHS reinforcement initially increased rapidly and then slightly decreased,

while both the corrosion potential (E_{corr}) and the pitting potential (E_b) underwent initial positive shifts followed by slight negative shifts. The appropriate concentration of sodium tungstate for this scenario was 0.1 g/L, for which the P_e was optimum at approximately 97.3%.

When sodium tungstate was added to the SCP solutions containing 3.5% NaCl, the tungstate ions played the following four roles: (1) The tungstate ions combined with Fe^{2+} to generate ferrous tungstate, which possesses an extremely low solubility and was incorporated into the corrosion products. (2) Fe^{2+} ions were oxidized to Fe^{3+} owing to oxidation by the tungstate ions. Thus, the film compactness and the protection by corrosion products such as $Fe(OH)_3$, Fe_2O_3, and ferric tungstate were enhanced [34–42,46]. (3) Tungstate ions with high valence were simultaneously reduced to WO_2 with lower valence, and these compounds were also incorporated into the corrosion products. WO_2 can improve the corrosion protection performance [47]. (4) The competitive adsorption of tungstate ions and chloride ions occurred and some chloride ions were displaced, thus reducing the corrosion damage to the passivation film by chloride ions. Owing to the combined effects of these four roles, the anodic polarization curves were greatly shifted to the left and exhibited a narrow passivation interval. The narrow passivation region indicates that the corrosion protection of FGHS reinforcement by sodium tungstate was limited. Moreover, the i_{corr} value increased with increasing sodium tungstate content. This may be attributable to the fact that the deposition of a tungstate film on the pitting will block diffusion of the corrosive solution out of the pitting hole, thus maintaining a relatively high corrosion in the holes and promoting pit growth. That is, the repassivation of the stable pits becomes difficult [46]. Moreover, tungstate only plays a role in membrane repair and is not a major component of the corrosion product film [37], resulting in an extremely low content of sodium tungstate inhibitor in the film.

The impedance diagrams for the FGHS samples immersed in SCP solutions containing 3.5% NaCl and various concentrations of sodium tungstate are presented in Fig. 4. In the presence of sodium tungstate inhibitor, the sizes of the impedance diagrams clearly increased (Fig. 4(a)). With increasing sodium tungstate concentration, the impedance initially greatly increased but then started to gradually decline. The responses of the impedance value at low frequency were also similar (Fig. 4(b)). The maximum impedance value was observed for sodium tungstate concentrations in the range of 0.1–0.3 g/L. After the addition of sodium tungstate, the peak value of the negative phase angle clearly increased and moved toward the low-frequency end, while the frequency range of the peak of the negative phase angle became wider (Fig. 4(b)).

The typical equivalent circuit depicted in Fig. 5 was used to analyze and fit the EIS diagrams shown in Fig. 4, where R_s is the solution resistance, CPE_c and R_c are the film capacitance and film resistance of the corrosion products on the surface of the FGHS reinforcement, respectively, and CPE_{dl} and R_{ct} are the double-layer capacitance and charge transfer resistance of the reinforcement/solution interface, respectively.

In actual electrochemical corrosion media, the corrosion product film and metal surface are inhomogeneous, and the film capacitance and double-layer capacitance will thus be different from ideal plate capacitance. Therefore, the Nyquist diagram will be deformed and the semicircle center will deviate from the real axis, and the peak value of the negative phase angle will also be smaller than 90°

[48–50]. A constant phase angle element (CPE) was used to characterize the actual capacitance and its impedance can be expressed as

$$Z_{\mathrm{CPE}} = 1/[Y_0(j\omega)^n]$$

The expression for n is as follows: $n = 1 - 2\alpha/180$, where α is the depression angle of the semicircle. If n equals 1, CPE is the capacitance. If n is 0, CPE is the resistance. If n is 0.5, CPE is the diffusion impedance. When n is in the range of 0 to 1, CPE indicates the dispersion effect of the double-layer capacitance or film capacitance [48,49].

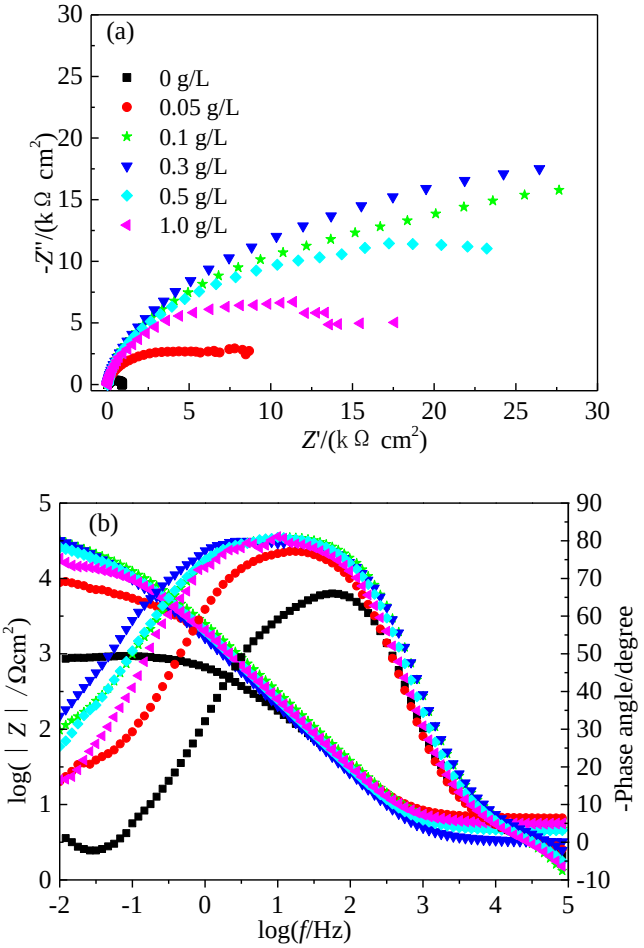

Figure 4. Effect of sodium tungstate concentration on (a) Nyquist and (b) Bode diagrams for FGHS reinforcement in SCP solutions containing 3.5% NaCl.

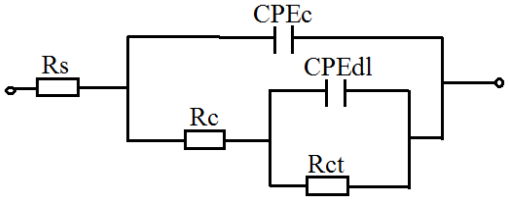

Figure 5. Equivalent circuit for FGHS reinforcement in SCP solutions containing 3.5% NaCl.

Figure 6 shows a comparison of the experimental and fitted EIS diagrams. The fitted diagram almost overlaps with the experimental data, with a fitting error of less than 5%. This indicates the feasibility of the equivalent circuit.

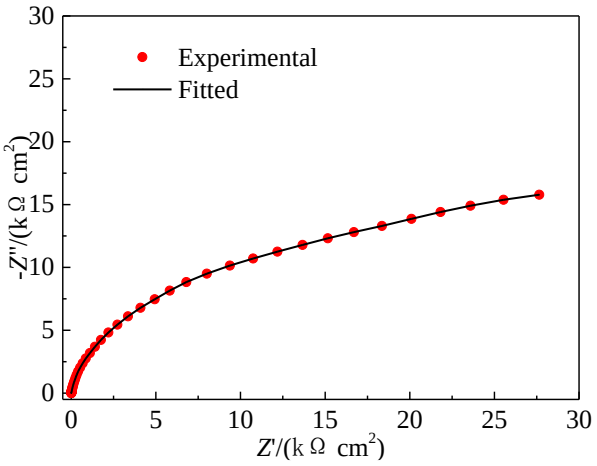

Figure 6. Comparison of the experimental and fitted EIS diagrams for FGHS reinforcement.

Table 2 shows the influence of various concentrations of sodium tungstate on the fitted parameters of the EIS diagrams for FGHS reinforcement. Upon the addition of sodium tungstate to the SCP solutions containing 3.5% NaCl, both R_c and R_{ct} increased significantly. The film resistance of the corrosion products and the charge transfer resistance of the electrochemical reaction were markedly enhanced.

Table 2. Effect of sodium tungstate concentration on the fitted parameters for FGHS reinforcement in SCP solutions containing 3.5% NaCl.

Sodium tungstate concentration/g L^{-1}	R_s/($\Omega \cdot cm^2$)	$Y_{0\text{-}c}$/($10^5\ \Omega^{-1} \cdot cm^{-2} \cdot s^{-n}$)	n_c	R_c/($k\Omega \cdot cm^2$)	$Y_{0\text{-}dl}$/($10^4\ \Omega^{-1} \cdot cm^{-2} \cdot s^{-n}$)	n_{dl}	R_{ct}/($k\Omega \cdot cm^2$)
0	5.7	10.8	0.892	0.31	2.68	0.282	0.64
0.05	6.7	4.50	0.905	4.75	2.63	0.550	9.36
0.1	5.0	3.56	0.921	12.70	0.63	0.505	70.55
0.3	5.4	2.52	0.905	17.23	0.34	0.612	45.83
0.5	4.6	4.42	0.920	11.30	0.71	0.521	37.41
1.0	5.8	4.52	0.912	9.65	1.12	0.363	23.54

As shown in Table 2, upon increasing the sodium tungstate concentration, both the film capacitance value ($Y_{0\text{-}c}$) and double-layer capacitance value ($Y_{0\text{-}dl}$) initially greatly decreased and then slightly increased. The reduction in the values was lower when the concentration of sodium tungstate was approximately 0.1–0.3 g/L. As is well known, the value of the capacitance is proportional to the dielectric constant and the surface area of the two plates and inversely proportional to the distance between the two plates. When a metal surface is covered with corrosion products, the dielectric constant decreases [48]. A more compact corrosion product film leads to a smaller surface area,

whereas a thicker corrosion product film results in a greater distance between the two plates. Moreover, upon the addition of sodium tungstate, the *n* value also increased but to various degrees. All of these points further imply the enhancement of the smoothness and flatness of the corrosion products on the surface of the FGHS reinforcement [51,52]. Therefore, the actual capacitance of the double layer and the corrosion product film on the surface of the FGHS reinforcement became closer to that for an ideal plate capacitance.

In general, passivation film and corrosion product films on the surfaces of metals possess semiconductor properties. Based on Mott–Schottky theory [43,44], the film is an *n*-type semiconductor when the slope of the Mott–Schottky curve is positive and a *p*-type semiconductor when the slope is negative. The carrier density N_D or N_A of the film can be calculated from the slope of the curve, and the flat-band potential E_{fb} can be obtained from the intercept.

The results for the influence of various concentrations of sodium tungstate on the Mott–Schottky curves of the corrosion product film on the FGHS reinforcement are presented in Fig. 7. Irrespective of whether sodium tungstate was present, the slopes for all of the Mott–Schottky curves were positive, demonstrating that the corrosion products on the surface of the FGHS reinforcement acted as an *n*-type semiconductor. Two line segments were observed in all of the Mott–Schottky curves. The straight line at low potential corresponds to a shallow donor density, which is associated with Fe^{2+} and oxygen vacancies, whereas the line at high potential corresponds to a deep donor density, which is related to Fe^{3+} and oxygen vacancies [53–55]. Both ions and vacancies in the corrosion products can participate in the charge transfer. A higher donor density N_D indicates a lower charge transfer resistance and a greater susceptibility of the metals to corrosion.

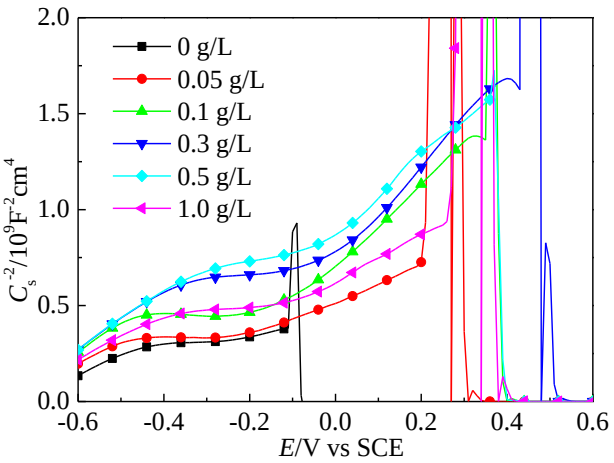

Figure 7. Effect of sodium tungstate concentration on the Mott–Schottky curves of the corrosion products on FGHS reinforcement.

As shown in Fig. 7, a discontinuous change occurred in the Mott–Schottky curves upon increasing the electrode potential beyond a particular value. This observation can be ascribed to the fact that an excessive electrode potential delays the conversion of Fe^{2+} to Fe^{3+} and depletes the donor density, thereby preventing the appearance of the characteristics of *n*-type semiconductors [56]. If the Fe^{3+} content of the film is low, the concentration of oxygen vacancies in the film will be high, thus leading to a large value of N_D and decreased protection by the corrosion product film [55–57].

Conversely, a higher Fe^{3+} content will afford better corrosion resistance. Therefore, if the electrode potential corresponding to the discontinuous change is high, the Fe^{3+} content of the film is also high and the corrosion resistance of the corrosion product film is enhanced.

Table 3 lists the semiconductor parameters of the corrosion products on the surfaces of the FGHS reinforcement samples. In the presence of sodium tungstate inhibitor, the $N_{D,1}$ and $N_{D,2}$ values decreased markedly, the $E_{fb,1}$ and $E_{fb,2}$ values clearly improved, and the discontinuous change in the electrode potential increased from −0.12 to 0.43 V *vs.* SCE. The optimal values of the indices were realized for sodium tungstate concentrations of approximately 0.1–0.3 g/L, which is consistent with the results of the microstructural observations, potentiodynamic polarization, and EIS measurements.

Table 3. Influence of sodium tungstate concentration on the semiconductor characteristics of the corrosion products for FGHS reinforcement in SCP solutions containing 3.5% NaCl.

Sodium tungstate concentration/g L^{-1}	Low-potential segment		High-potential segment		Potential of discontinuous change/V *vs.* SCE
	$N_{D,1}$/(×10^{20} cm^3)	$E_{fb,1}$/V *vs.* SCE	$N_{D,2}$/(×10^{19} cm^3)	$E_{fb,2}$/V *vs.* SCE	
0	2.03	−0.980	—	—	−0.12
0.05	1.14	−0.790	13.2	−0.565	0.20
0.1	0.803	−0.772	5.69	−0.330	0.35
0.3	0.830	−0.792	4.68	−0.272	0.43
0.5	0.822	−0.790	5.78	−0.408	0.36
1.0	1.13	−0.813	9.79	−0.500	0.29

3.2 Influence of tungstate/tartrate mixed inhibitor on FGHS reinforcement corrosion inhibition

Based on the above results, sodium tungstate exhibits an inhibitory effect on the corrosion of FGHS reinforcement in SCP solutions containing 3.5% NaCl. The electrochemical corrosion indices were improved. However, sodium tungstate alone cannot completely mitigate the corrosion of FGHS reinforcement. Recently, tungstate mixed inhibitor for carbon steel and stainless steel have been studied and the results demonstrated that the corrosion resistance of the alloys was enhanced [38–40]. The use of tartrate alone accelerates the corrosion of carbon steel, and the inhibitory effect of tungstate is limited [41]. However, a synergistic corrosion resistance effect due to improved passivation occurs when these two chemicals are combined in a 1:1 ratio [41]. In this study, a mixed inhibitor based on sodium tungstate/sodium tartrate in a ratio of 1:1 was reexamined, and the results are presented in Fig. 8.

As shown in Fig. 8(a), the anodic polarization curves for the FGHS reinforcement samples in the presence of the different corrosion inhibitors decreased (i.e., shifted from right to left) in the following order: without inhibitor >> with tartrate inhibitor > with tungstate inhibitor ≈ with mixed inhibitor. Furthermore, the cathodic curves decreased in the following order: without inhibitor ≈ with tungstate inhibitor > with tartrate inhibitor ≈ with mixed inhibitor. To a first approximation, the anodic polarization curve in the presence of the mixed inhibitor could be overlaid with that in the presence of the tungstate inhibitor, while the cathodic curve for the former case almost coincided with that for the

tartrate inhibitor. As shown in Fig. 8(b), the electrochemical impedance of the FGHS reinforcement in the presence of the mixed inhibitor was markedly greater than that in the presence of either tungstate or tartrate inhibitor alone. Based on the combined results of Figs. 8(c) and 2(c), the addition of the mixed inhibitor further reduced pit formation on the surface of the FGHS reinforcement.

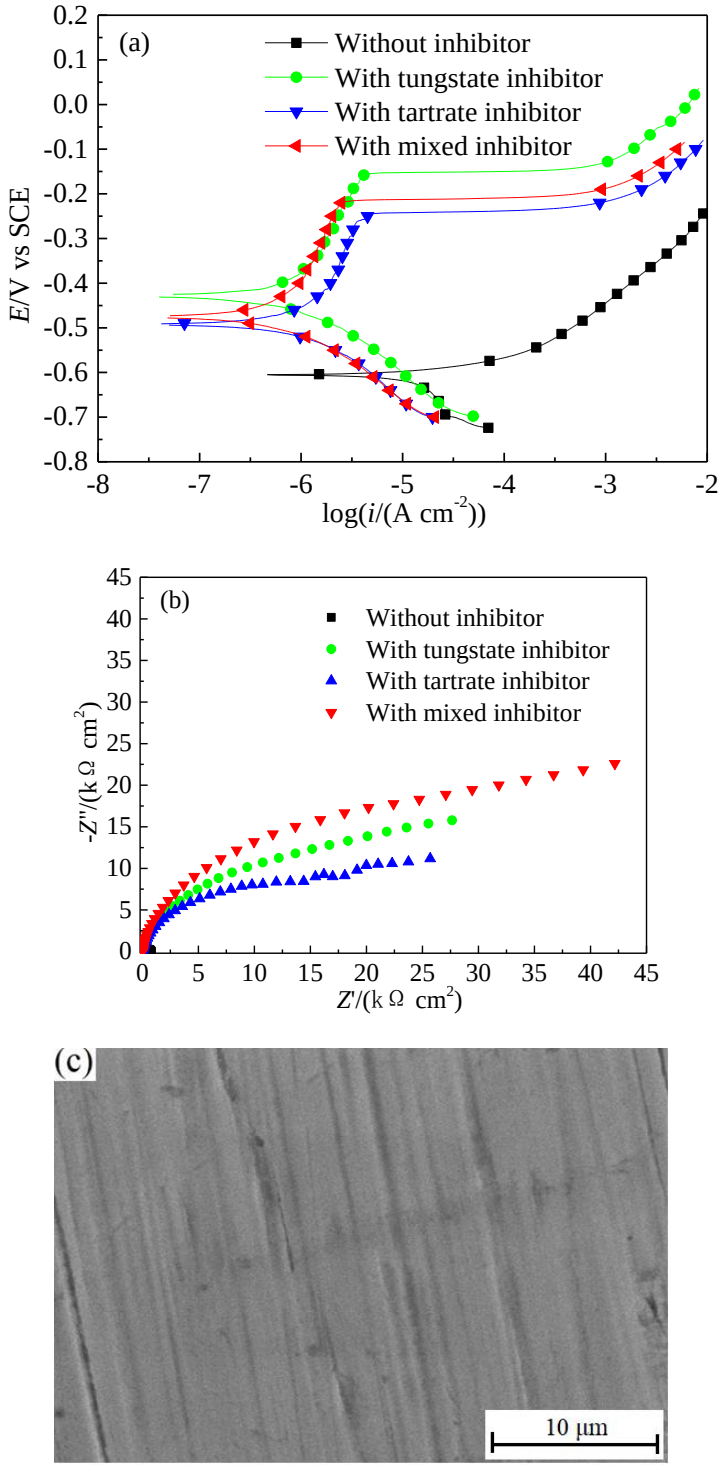

Figure 8. Effect of the tungstate/tartrate mixed inhibitor on (a) the polarization curves, (b) the EIS spectra, and (c) the microstructure of FGHS reinforcement in SCP solutions containing 3.5% NaCl.

However, the degree to which the anodic polarization curve for the FGHS reinforcement shifted to the left in the presence of the mixed inhibitor was less than the sum of the shifts observed for the single inhibitors, and the impedance in the presence of the mixed inhibitor was also less than the sum of those of the single inhibitors. These results indicate that although the mixed inhibitor still affords advantages over the use of the single inhibitors in terms of enhancing the corrosion resistance, no synergistic effect of corrosion inhibition was observed for the mixed inhibitor in SCP solution containing 3.5% NaCl.

3.3 Corrosion comparison for FGHS and HPB300 reinforcement

The effects of the sodium tungstate and mixed inhibitor on the polarization curves and EIS spectra were investigated for FGHS and HPB300 reinforcement and the results are compared in Fig. 9. SEM images showing the corrosion microstructures of the HPB300 steel samples are also presented in Fig. 10.

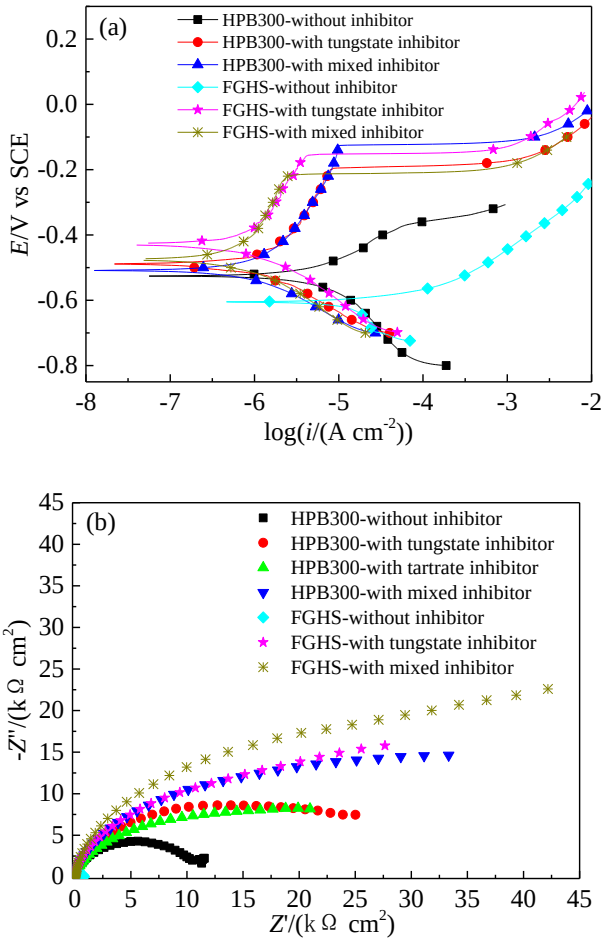

Figure 9. Effects of inhibitors on (a) the polarization curves and (b) the EIS spectra for HPB300 and FGHS reinforcement.

As shown in Fig. 9(a), in the presence of the sodium tungstate inhibitor, the cathodic polarization curve for the HPB300 sample moved slightly to the left, whereas the anodic curve clearly

shifted to the left. The anodic corrosion process for the HPB300 sample was significantly inhibited by tungstate and the cathodic process was also hindered. Upon the addition of the mixed inhibitor, the anodic polarization curve was very similar to that upon the addition of the tungstate inhibitor, whereas the cathodic curve slightly shifted to the left. Only a very limited improvement in the corrosion resistance was observed for the mixed inhibitor in the case of the HPB300 sample.

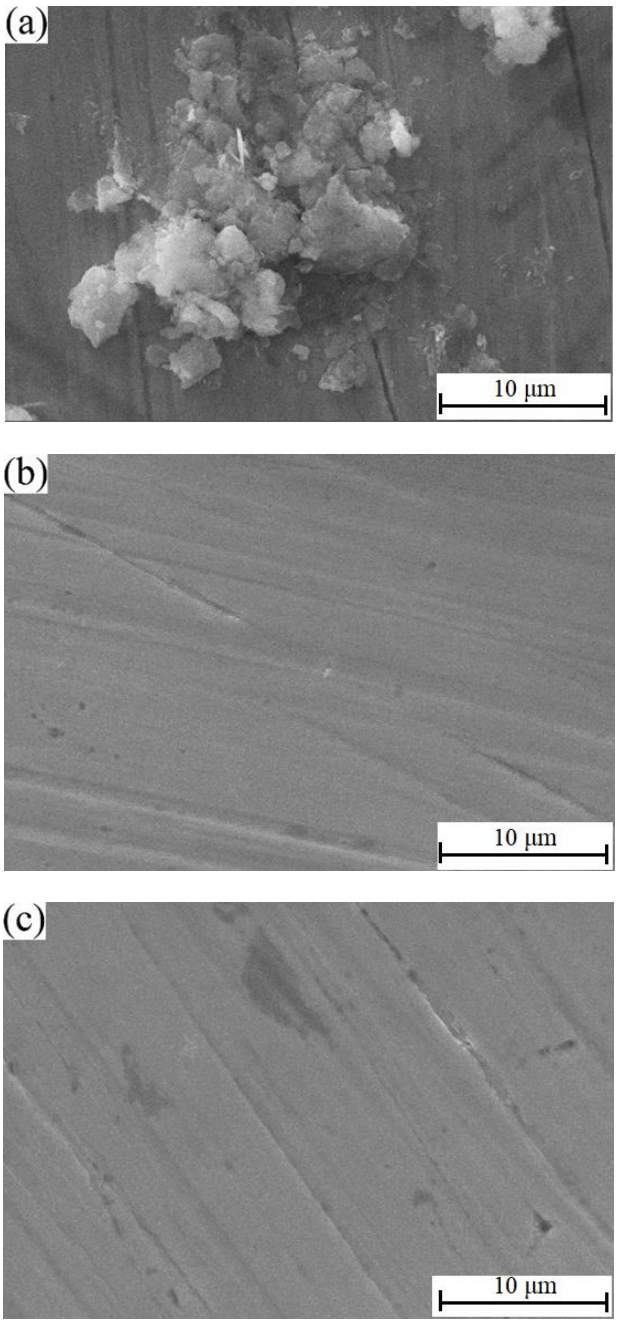

Figure 10. Corrosion morphology of HPB300 reinforcement after immersion in SCP solutions containing 3.5% NaCl: (a) without inhibitor, (b) with tungstate inhibitor, (c) with tungstate/tartrate mixed inhibitor.

From inspection of Fig. 9(b), it can be seen that the electrochemical impedance for the HPB300 sample increased as follows: without inhibitor < with tartrate inhibitor < with tungstate inhibitor < with

mixed inhibitor. However, the electrochemical impedance in the presence of the mixed inhibitor was lower than the sum of those in the presence of the two single inhibitors, again suggesting the absence of a synergistic effect in the case of the mixed inhibitor. These results, together with the images of the corrosion microstructures shown in Fig. 10, suggest that the corrosion of HPB300 steel was clearly inhibited by the addition of the mixed inhibitor. However, the observed morphologies of the HPB300 steel samples were almost the same irrespective of whether a single or mixed inhibitor was used, with only a small number of corrosion pits observed. This implies that both the tungstate inhibitor and the tungstate/tartrate mixed inhibitor were able to improve the corrosion resistance of the HPB300 samples, although no synergistic effects occurred for the mixed inhibitor. This result is similar to that obtained for the FGHS samples.

The differences in the corrosion behavior of the HPB300 and FGHS reinforcement samples were further considered. As shown in Fig. 9, in the absence of a corrosion inhibitor, the cathodic polarization curves of the two samples were approximately identical, although the anodic curve for the HPB300 steel sample was shifted to the left compared with that for the FGHS sample. The electrochemical impedance of the former was also clearly greater than that of the latter and the corrosion damage to the HPB300 sample surface was clearly less than that to the FGHS sample surface. That is, the corrosion mediated by the chloride ions was greater for the FGHS reinforcement than for the HPB300 reinforcement. In the presence of the sodium tungstate inhibitor, the cathodic polarization curve for the HPB300 sample was slightly shifted to the left of that for the FGHS sample. However, the anodic curve of the former was clearly to the right of that of the latter, and the electrochemical impedance of the former was also less than that of the latter. All of these results indicate that the addition of sodium tungstate leads to a smaller improvement in corrosion resistance for HPB300 than for FGHS. In other words, sodium tungstate exerts a greater corrosion inhibition effect on FGHS reinforcement than on HPB300 reinforcement. This finding is quite different from the corrosion inhibition results observed for nitrate, phosphate, D-gluconate, diisooctyl sebacate, and phytic acid, which were found to be more effective for HPB300 reinforcement [17,18,58,59]. Moreover, the corrosion inhibition effect of the tungstate/tartrate mixed inhibitor on HPB300 reinforcement was also found to be inferior to that on FGHS reinforcement. The differences in the corrosion resistance mechanisms of these inhibitors will be the subject of further study.

4. CONCLUSIONS

(1) The corrosion inhibition effect of sodium tungstate inhibitor on FGHS reinforcement in SCP solutions containing 3.5% NaCl was investigated, and the corrosion inhibition by a tungstate/tartrate mixed inhibitor was also examined. Furthermore, the inhibition effects were compared for HPB300 reinforcement and FGHS reinforcement.

(2) Upon increasing the sodium tungstate concentration (0 to 1.0 g/L), the electrochemical impedance of the FGHS samples increased greatly and then slightly decreased, while the donor density of the corrosion products and the corrosion current density initially decreased rapidly and then slightly increased. The optimum concentration of sodium tungstate was approximately 0.1–0.3 g/L. The

corrosion products on the surfaces of the FGHS samples were compact and only a few corrosion pits were evident.

(3) The tungstate/tartrate mixed inhibitor retained the advantages of the single inhibitor, although no synergistic effects were observed.

(4) In the absence of inhibitor, the corrosion resistance indices for the FGHS samples were clearly inferior to those for the HPB300 samples, but tungstate alone or the tungstate mixed inhibitor conferred superior corrosion resistance to the FGHS samples compared with the HPB300 samples.

ACKNOWLEDGMENTS

This work was supported by the National Natural Science Foundation of China (Nos. 51578255 and 51778247), the Natural Science Foundation of Fujian Province (No. 2017J01489), and the Program for the Innovative Research Team in Science and Technology in Fujian Province University.

References

1. A. B. Araz, F. Li, R. T. Patricia, D. Ponge and D. Raabe, *Mater. Sci. Eng., A*, 463 (2006) 138.
2. A. I. Zaky, A. El-Morsy and T. El-Bitar, *J. Mater. Process. Technol.*, 209 (2009) 1565.
3. C. F. Yang and Q. L. Wang, *J. Iron Steel Res. Int.*, 15 (2008) 81.
4. J. Ścigałło and G. M. Teresa, *Procedia Eng.*, 172 (2017) 953.
5. J. Z. Xiao, Y. Z. Hou and Z. F. Huang, *Fire Saf. J.*, 69 (2014) 23.
6. W. J. Ge, J. W. Zhang, D. F. Cao and H. Dai, *J. Civ. Archit. Environ. Eng.*, 35 (2013) 38.
7. D. Song, A. B. Ma, W. Sun, J. H. Jiang and G. H. Guo, *Corros. Sci.*, 82 (2014) 437.
8. M. A. Islam, *Procedia Eng.*, 125 (2015) 623.
9. H. Torbati-Sarraf and A. Poursaee, *Constr. Build. Mater.*, 167 (2018) 680.
10. M. Gong, Z. X. Yu and L. Chen, *Metal Corrosion Theory and Corrosion Control*, Chemistry Industry Press, Beijing, 2009.
11. K. K. Sharma, R. N. Deo, A. Kumar and K. Mamun, *Constr. Build. Mater.*, 165 (2018) 533.
12. J. Ahlström, J. Tidblad, B. Sederholm and L. Wadsö, *Mater. Corros.*, 67 (2016) 1049.
13. A. P. Montaño, J. S. Montero, C. Andrade, J. Fullea, E. Moreno and V. Matres, *Constr. Build. Mater.*, 186 (2018) 495.
14. B. L. Lin and Y. Y. Xu, *J. Zhenzhou Univ. Light Ind. (Natural Sci.)*, 25 (2010) 45.
15. J. J. Shi, W. Sun and G. Q. Geng, *Acta Metall. Sin.*, 47 (2011) 449.
16. J. J. Shi, W. Sun, G. Q. Geng and J. Y. Jiang, *J. Univ. Sci. Technol. B.*, 33 (2011) 1471.
17. B. L. Lin, C. N. Liu, Z. Luo, J. D. Li, S. Wang and Y. Y. Xu, *Int. J. Electrochem. Sci.*, 12 (2017) 2070.
18. B. L. Lin and Y. Y. Xu, *Int. J. Electrochem. Sci.*, 11 (2016) 3824.
19. B. L. Lin and Y. Y. Xu, *Int. J. Electrochem. Sci.*, 14 (2019), 75.
20. C. N. Cao, *Principle of Electrochemical Corrosion*, Chemistry Industry Press, Beijing, 2018.
21. H. S. Lee, H. M. Yang, J. K. Singh, S. K. Prasad and B. Y. Yoo, *Constr. Build. Mater.*, 173 (2018) 443.
22. S. Tsouli, A. G. Lekatou, S. Kleftakis, T. E. Matikas and P. T. Dalla, *Procedia Struct. Integr.*, 10 (2018) 41.
23. M. A. Asaad, M. Ismail, M. M. Tahir, G. F. Huseien and Y. P. Asmara, *Constr. Build. Mater.*, 188 (2018) 555.
24. B. Q. Dong, W. J. Ding, S. F. Qin and S. X. Hong, *Cem. Concr. Comp.*, 85 (2018) 83.
25. R. A. Celeste and V. A. Idalina, *Electrochim. Acta*, 49 (2004) 2779.
26. Q. Qu, L. Li, W. Bai, S. Jiang and Z. Ding, *Corros. Sci.*, 51 (2009) 2423.

27. M. A. Deyab and S. S. Abd Elrehim, *Electrochim. Acta*, 53 (2008) 1754.
28. W. D. Robertson, *J. Electrochem. Soc.*, 98 (1951) 94.
29. J. A. Torre and A. Arevalo, *Bol. Inst. Espam. Oceanogr.*, 46 (1951) 27.
30. K. K. Chew and D. R. Gabe, *Corros. Prev. Control*, 26 (1979) 5.
31. E. A. Lizolvs, *J. Electrochem. Soc.*, 114 (1979) 1015.
32. J. M. Abd El Kadar, A. A. Warraky and A. M. Abd El Aziz, *Br. Corros. J.,* 33 (1998) 39.
33. V. S. Sastri, C. Tjan and P. R. Roberge, *Br. Corros. J.*, 26 (1991) 251.
34. E. Fujioka, H. Nishihara and K. Aramaki, *Corros. Sci.*, 38 (1996) 1915.
35. G. N. Mu, X. H. Li, Q. Qu and J. Zhou, *Corros. Sci.*, 48 (2006) 445.
36. S. Z. E. Abedin, *J. Appl. Electrochem.*, 31 (2001) 711.
37. X. H. Liu, J. Han, C. Y. Sun and Q. H. Wang, *Surf. Technol.*, 40 (2011) 52.
38. M. C. Scholant, E. F. Coutinho, S. P. Dias, D. S. Azambuja, S. N. Silva and S. M. Tamborim, *Surf. Interface Anal.*, 47 (2015) 192.
39. S. M. A. Shibli and V. S. Saji, *Corros. Sci.*, 47 (2005) 2213.
40. M. Sharma, A. V. R. Kumar and N. Singh, *Trans. Indian Inst. Met.*, 61 (2008) 251.
41. B. Jabeera, S. M. A. Shibli and T. S. Anirudhan, *Appl. Surf. Sci.*, 252 (2006) 3520.
42. Z. Lu, S. Z. Zheng, Y. C. Zhu, *J. East China Inst. Chem. Technol.*, 5 (1982) 403.
43. A. Fattah-alhosseini and S. Vafaeian, *J. Alloys Compd.*, 639 (2015) 301.
44. I. M. Gadala and A. Alfantazi, *Appl. Surf. Sci.*, 357 (2015) 356.
45. K. Aramaki and T. Shimura, *Corros. Sci.*, 52 (2010) 1464.
46. H. Y. Shi and Y. Zuo, *Corros. Sci. Prot. Technol.*, 30 (2018) 167.
47. C. Y. Tsai, J. S. Liu, P. L. Chen and C. S. Lin, *Surf. Coat. Technol.*, 205 (2011) 5124.
48. C. N. Cao and J. Q. Zhang, *An Introduction to Electrochemical Impedance Spectroscopy*, Science Press, Beijing, 2004.
49. L. H. Jiang, G. H. Huang, J. X. Xu, Y. R. Zhu and L. L. Mo, *Constr. Build. Mater.*, 30 (2012) 516.
50. D. Weng, P. Jokiel, A. Uebleis and H. Boehni, *Surf. Coat. Technol.*, 88 (1997) 147.
51. A. V. Benedetti, P. T. A. Sumodjo, K. Nobe, P. L. Cabot and W. G. Proud, *Electrochim. Acta*, 40 (1995) 2657.
52. M. Cao, L. Liu, Z. F. Yu, L. Fan and F. H. Wang, *J. Mater. Sci. Technol.*, 35 (2019) 651.
53. J. Luo, Y. Wang, J. B. Jiang, Q. D. Zhong, Z. Y. Zhu and L. Zhang, *Acta Chim. Sin.*, 70 (2012) 1213.
54. X. G. Chen, Y. Yang, Z. G. Lin, W. Chu, Y. X. Shi and B. M. Wei, *Appl. Surf. Sci.*, 103 (1996) 189.
55. J. S. Kim, E. A. Cho and H. S. Kwon, *Corros. Sci.*, 43 (2001) 1403.
56. X. Zhou, H. Y. Yang and F. H. Wang, *Corros. Sci. Prot. Technol.*, 22 (2010) 343.
57. W. Chen, R. G. Du, R. G. Hu, H. Y. Shi, Y. F. Zhu and C. J. Lin, *Acta Metall. Sin.*, 47 (2011) 735.
58. B. L. Lin, Z. Luo, C. N. Liu, X. F. Liu and Y. Y. Xu, *Int. J. Electrochem. Sci.*, 12 (2017) 8892.
59. B. L. Lin and Y. Y. Xu, *J. Build. Mater.*, 19 (2016) 1082.

© 2019 The Authors. Published by ESG (www.electrochemsci.org). This article is an open access article distributed under the terms and conditions of the Creative Commons Attribution license (http://creativecommons.org/licenses/by/4.0/).